Multidisciplinary Optimization of a Transonic Truss Braced Wing Aircraft with Hybrid-Electric Propulsion

Mark K. Leader*, Eliot Aretskin-Hariton, and Kenneth T. Moore†
NASA Glenn Research Center, Cleveland, OH, USA

Next generation aircraft concepts have subsystems that are increasingly inter-connected. This necessitates advanced design tools using gradient based optimization to properly account for strong subsystem coupling in these aircraft. Additionally, these design tools require accurate modeling capability to support the increased interest in electrified propulsion. Design studies for these aircraft must consider the trade-offs between electric propulsion and turbojet engines at all points in the flight envelope to determine the optimal balance between propulsion options. This paper describes the development of an electric propulsion subsystem model designed to work within Aviary - an open source aircraft design tool. We will demonstrate the electric propulsion model operating with Aviary by showing results from an optimized Transonic Truss-Braced Wing (TTBW) concept using assisted electric propulsion during climb. First, we present results with and without electrification to show the overall system impacts of hybrid electric propulsion during climb. We also present two distinct battery models compatible with this optimization framework, and compare results using both. Next, we ran the same problem using a slightly different cell type, and demonstrate a considerable change in the result. Finally, we vary the cell energy density of the batteries, and provide an illustrative trend for the system-level impact for improving cell technology.

*mark.leader@nasa.gov, AIAA Member
†Banner Quality Management Inc.

Nomenclature

Acronyms

CED	Cell energy density (Wh/kg)
C_{Thev}	Thevenin equivalent capacitance
E_{con}	Energy constraint
E_{nom}	Nominal battery energy available
E_{req}	Total energy required by the mission
GTOW	Gross Takeoff Weight
I	Current (A)
I_{max}	Max current during the mission (A)
I_{cell}	Cell maximum continuous discharge rating (A)
I_{line}	Line current (A)
k	Scalar to ensure remaining state of charge
m	Mass (kg)
n_{p}, $n_{\text{p,2}}$	Number of cells in parallel
n_{s}	Number of cells in series
P_{in}	Power in to the motor (from the battery) (W)
P_{out}	Power out from the motor (to the shaft) (W)
P_{max}	Max motor power during the mission (W)
Q_{max}	Cell energy capacity (Ah)
R_0	Ohmic resistance
R_{Thev}	Polarization resistance
SLS	Sea Level Static
SOC	State-of-charge (%)
t	Time
T	Temperature (K)
TOC	Top of Climb
TTBW	Transonic Truss-Braced Wing
U_{oc}	Open-circuit voltage (V)
V_{battery}	Nominal pack voltage (V)
$V_{\text{cell,low}}$	Cell discharge cutoff voltage (V)
$V_{\text{cell,nominal}}$	Nominal cell voltage (V)
V_{line}	Line voltage (V)
$w_{\text{frac,case}}$	Weight fraction of the case relative to the total cell weight
XDSM	eXtended Design Structure Matrix
η	Efficiency (%)

Subscripts

Battery	The aggregate battery subsystem
Cell	An individual battery cell
Case	The casing material enclosing the cells
Conv	Voltage converter
Motor	The electric motor subsystem
Pack	An individual assembly of a battery case with cells

I. Introduction

Electrification is becoming an increasing demand for aircraft concepts, and novel conceptual design tools are needed to support their development. Notably, future commercial transport aircraft are trending towards increasingly coupled subsystems, and that is even more the case when electric propulsion is involved. To be useful for these applications, conceptual design tools need to evaluate and optimize electric propulsion system performance over the duration of a mission.

Previous work has been done in the area of aircraft conceptual design including electric propulsion [1–3]. In this work, we developed an electric propulsion external subsystem to work with Aviary [4], an open-source aircraft conceptual design tool, to explore hybrid-electric or fully-electric aircraft concepts. We expand upon the hybrid electric concept for the Transonic Truss-Braced Wing (TTBW) aircraft presented in Aretskin-Hariton et al. [3]. This work examines the system-level impacts of electric propulsion on the TTBW concept vehicle, using a fixed amount of electric power during climb. Several subsystems impact the aircraft's performance objectives, many of which are coupled with other subsystems, so modeling each of these relevant subsystems is a priority for this work. This allows us to accurately model subsystem interactions and trade-offs at the aircraft system level. Furthermore, it is desirable to simultaneously optimize the aircraft subsystems and the aircraft's mission, as the two are strongly coupled, which is what Aviary allows us to do.

In Section II, we describe the methodology used for the conceptual design optimization problem, including detailed descriptions of the battery (II.A) and motor models (II.B). In Section III, we present the optimization results of the TTBW aircraft, including a baseline case without electrification, and three different cases with partially electrified propulsion during climb. We also present results varying cell energy density to illustrate the impact of improving cell technology. Finally, we summarize conclusions in Section IV and suggest topics for future work.

II. Methods

The emphasis of this work is using gradient-based optimization to analyze aircraft concepts with partially-electrified propulsion. To do this, we focus on extending the capability of state-of-the-art aircraft optimization tools, namely Aviary [4]*. Aviary is an open-source tool for multidisciplinary design, analysis, and optimization of aircraft concepts. Aviary is written in Python using OpenMDAO† [5] to efficiently compute total derivatives from analytic partial derivatives, and also uses Dymos‡ [6] to solve the mission partial differential equations and optimize the aircraft trajectory. As Aviary is built using OpenMDAO, it supports a wide range of optimizers; in this work, we use the Sparse Nonlinear Optimizer (SNOPT) [7].

Aviary includes a number of aircraft subsystems natively (e.g. propulsion, aerodynamics, weight, and more), but also has the flexibility to support user-defined subsystems, either to replace the native Aviary subsystems with more accurate or higher fidelity anlyses, or to expand the scope of the design outside of Aviary's standard support. This work utilizes that feature (referred to as "External Subsystems") to evaluate aircraft concepts that include electric propulsion; the details of this model will be described in the following Sections (II.A and II.B).

Within the electric propulsion subsystem model, some calculations are done prior to simulating the mission and are static with respect to time, whereas other variables depend on time - such as, but not limited to, controls or state variables. In Aviary nomenclature, and throughout the remainder of this paper, the prior values will be referred to as *Pre-Mission*, and the latter values are referred to as *Mission*. (Aviary also supports *Post-Mission* calculations, but none are relevant for this work.)

Overall, the electric propulsion external subsystem contains a battery and a motor model. A voltage converter is also used, but we will consider it part of the motor model and describe it as such. The battery and motor models include both Pre-Mission and Mission calculations. Two version of the electrical subsystem and presented in this work, known as the "basic" and "advanced" electrical models. The battery model is different between the two, while the motor model is constant, and only treated slightly different to support the different connections to the battery model.

Figures 1 and 2 show the electrical-propulsion subsystem eXtended Design Structure Matrix (XDSM) [8] for the basic and advanced electrical subsystem models, respectively. The XDSM shows these components at a high level, with model inputs across the top, outputs to the right, and how variables interact between components.

Starting with the basic electrical model in Figure 1, the Battery Pre-Mission component takes in nominal energy as a design variable from the optimizer to size the pack and compute the mass of the battery pack. The Motor Pre-Mission

*https://github.com/OpenMDAO/Aviary

†https://openmdao.org

‡https://openmdao.github.io/dymos/

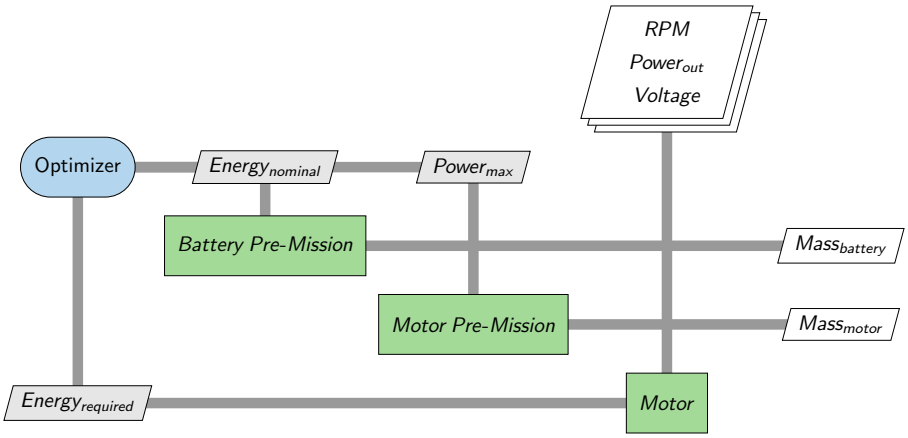

Fig. 1 Electrical-propulsion subsystem eXtended Design Structure Matrix (XDSM) for the basic electrical model. Outputs to the right are made available to the optimizer and made available to the user for graphing.

component simply takes in one design variable, maximum power, and computes the mass of the electric motors. The Motor Mission component takes in RPM and total power output as values connected from the propulsion subsystem. The power from the Motor Mission is used to integrate the energy required by the battery pack, so it is fed back in to the optimizer to be constrained with nominal energy.

Next for the advanced electrical model shown in Figure 2, in the Battery Pre-Mission component, nominal pack voltage is an input parameter; maximum current and cell discharge rate are both design variables for the optimizer and are inputs to Battery Pre-Mission. Battery Pre-Mission computes the number of cells in series and in parallel for the pack (n_s, and n_p, respectively), as well as the total mass of the pack, which are passed as inputs to the Battery Mission component. The Motor Pre-Mission and Mission components are nearly identical to the basic electrical subsystem, except for how it couples with the advanced battery model, which requires two-way coupling with current and voltage. The battery and motor models will be described in detail in the following sections (II.A, II.B).

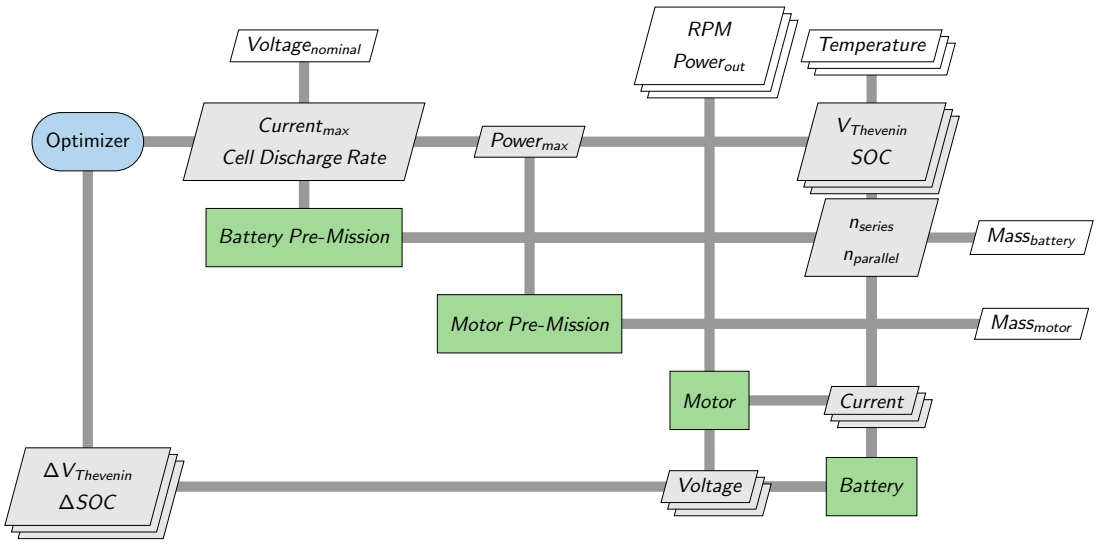

Fig. 2 Electrical-propulsion subsystem eXtended Design Structure Matrix (XDSM) for the advanced electrical model. Outputs to the right are made available to the optimizer and made available to the user for graphing.

A. Battery Model

In this work, we will present two different approaches to battery subsystem analysis: a "basic" model, and an "advanced" model. The methodology for these two models is presented in Sections II.A.1 and II.A.2, respectively. Results using both model types are compared in Section III.A.

1. Basic Battery Model

The basic battery model is intended to resemble the behavior of the advanced model, while being easier to set up. We have also found that the optimizer finds a good result in fewer iterations using this approach, and more reliably. The disadvantage of this model is that more assumptions are required, and also not all of the pack sizing constraints can be considered using this approach.

The basic battery model does not use any cell-level data, nor does it integrate any state variables at the cell level like we do in the advanced battery model. For the basic battery model, an initial and final pack voltage value are assumed. In this work, we use an initial value of 900 Volts, and a final value of 700 Volts. A linearly decreasing trend is acceptable, because voltage will drop as state-of-charge decreases. For the basic model, the battery pack is sized to meet the required energy demand (kWh) for the mission. A scalar state variable for energy required, E_{req}, is integrated over the duration of the mission with power in to the motor (output from the battery pack), P_{in}, as the rate source for the integration. P_{in} is fully controlled by the motor subsystem, and is a function of the motor power output (to the turbojet shaft), P_{out}, and the motor and converter efficiencies. The total energy required is used in an energy balance constraint

$$E_{\text{con}} = E_{\text{nom}} - kE_{\text{req}} \geq 0, \tag{1}$$

where E_{nom} is a design variable representing the nominal battery energy, and k is a scalar to ensure residual state of charge at the end of the mission, which we set to 1.2 in this work to ensure 20% state of charge remaining at the end of the mission. Finally, the mass of the battery pack can be determined based on the nominal energy of the battery pack, with

$$m_{\text{battery}} = n_{\text{packs}} E_{\text{nom}} / CED, \tag{2}$$

where n_{packs} is an integer multiplier for the number of battery packs on the aircraft, which in this case is two: one per motor, and one motor per turbojet engine. Finally, CED is the overall cell energy density of the battery pack.

2. Advanced Battery Model

The advanced battery model is a cell-level model based on previous work by Chin et al. [1]. Their model uses experimental cell discharge data to fit a Thevenin voltage open-circuit model to solve an ordinary differential equation (ODE) for state-of-charge (SOC) and Thevenin voltage as a function of cell temperature:

$$U_{\text{oc}}, C_{\text{Thev}}, R_0, R_{\text{Thev}} = f\left(SOC, T_{\text{battery}}\right) \tag{3}$$

where U_{oc} is the open-circuit voltage, C_{Thev} is the Thevenin equivalent capacitance, R_0 is the Ohmic resistance, and R_{Thev} is the polarization resistance. The cell-level parameters from Eq. 3 are computed using a basic linear interpolation provided in OpenMDAO. Further details of the cell-level model can be found in Chin et al. [1].

The battery subsystem computes certain parameters prior to simulating a mission ("Pre-Mission") while others are computed with respect to time during a mission ("Mission"). In Pre-Mission, the battery pack sizing takes place. Specifically, the Pre-Mission battery component calculates the number of cells in series and parallel (n_{s}, n_{p}), given as:

$$n_{\text{s}} = \frac{V_{\text{battery}}}{V_{\text{cell, low}}} \tag{4}$$

$$n_{\text{p}} = \frac{I_{\text{max}}}{I_{\text{cell}}} \tag{5}$$

$$n_{\text{p,2}} = n_{\text{p}} \left(\frac{E_{\text{req}}}{E_{\text{nom}}}\right) \tag{6}$$

The number of cells in series and parallel are also used to compute total pack mass, m_{battery}. These calculations depend on two design variables: cell discharge rate, I_{cell}, and an estimate of the peak current draw during the mission, I_{max}. The estimate of the peak current draw, I_{max}, is used as a slack variable in the optimization with a constraint such

that: $I_{\max} \geq \max(\mathbf{I})$. The optimizer will be incentivized to make the two sides of the inequality constraint roughly equal with any choice of objective function related to aircraft weight (e.g. gross take-off weight or fuel burn). The number of cells in series, n_s, is based on nominal pack voltage, V_{battery}, which is a fixed input. Two values are computed for n_p; n_p and $n_{p,2}$. n_p is based on the peak power estimated for the mission, $I_{\max}$. $n_{p,2}$ is based on the total energy required by the mission. $n_{p,2}$ is defined to be equal to n_p times a proportionality factor of E_{req} divided by E_{nom}, where E_{req} is the total energy required for the mission, and is computed by integrating over time the total power output from the battery pack, while E_{nom} is the total amount of energy (in kWh) that the battery pack has available. There is a constraint on the optimization that $n_{p,2} = n_p$, requiring that both the max-current constraint and the required energy constraint are simultaneously satisfied.

These Pre-Mission battery calculations also depend on a number of fixed cell and pack parameters, including: cell mass, m_{cell}, total number of packs on the aircraft, n_{packs}, low cell voltage, $V_{\text{cell, low}}$ (defined as the discharge cut-off voltage), nominal cell voltage, $V_{\text{cell, nominal}}$, cell energy capacity, E_{cell}, total energy required, E_{req}, case weight fraction, $w_{\text{frac,case}}$, and nominal pack voltage, V_{battery}.

The Mission-based battery analysis primarily serves to integrate the state variables ($\mathbf{V}_{\text{Thev}}$, $\mathbf{SOC}$) and compute the time-varying pack voltage, $\mathbf{V}$. The state variables (along with cell temperature, T) are inputs to a linear interpolation of tabular data returning cell parameters (U_{oc}, C_{Thev}, R_0, R_{Thev}) for the Thevinin equivalent circuit model. These values are then all used to compute the rates of the state variables ($\frac{\mathrm{d}\mathbf{V}_{\text{Thev}}}{\mathrm{d}t}$, $\frac{\mathrm{d}\mathbf{SOC}}{\mathrm{d}t}$), as well as total pack voltage $\mathbf{V}$. The rate of change of Thevenin voltage is computed as:

$$\frac{\mathrm{d}\mathbf{V}_{\text{Thev}}}{\mathrm{d}t} = \frac{\mathbf{I}_{\text{line}}}{3600 \times Q_{\max}} \tag{7}$$

where $\mathbf{I}_{\text{line}} = \mathbf{I}/n_p$ is the line current, $Q_{\max}$ is the cell energy capacity in Amp-hours, and the "3600" term converts "hours" to "seconds". The rate of the change of state-of-charge is given as:

$$\frac{\mathrm{d}\mathbf{SOC}}{\mathrm{d}t} = -\frac{\mathbf{V}_{\text{Thev}}}{R_{\text{Thev}} C_{\text{Thev}}} + \frac{I_{\text{line}}}{C_{\text{Thev}}} \tag{8}$$

and the total pack voltage is computed as:

$$\mathbf{V} = \mathbf{V}_{\text{line}} n_s \tag{9}$$

where $\mathbf{V}_{\text{line}} = \mathbf{I}_{\text{line}} (R_0 \mathbf{I}_{\text{line}} + \mathbf{V}_{\text{Thev}})$ is the line voltage. The mission-level battery calculations can be vectorized because of the collocation approach that Dymos uses to compute the time-varying state values. The time-varying pack voltage is fed into the motor subsystem to evaluate electric motor power demanded and the resulting current draw on the battery pack.

B. Motor Model

The only value computed in Pre-Mission for the motor component is the motor mass, m_{motor}. The motor mass uses an estimate of the maximum motor power over the mission, $P_{\max}$. $P_{\max}$ is used as a slack variable during optimization with a constraint enforced such that $P_{\max} \geq \max(\mathbf{P}_{\text{out}})$, where $\mathbf{P}_{\text{out}}$ is the vector of power output from the motor during the mission. The mass of the motor is estimated using a simple linear interpolation on known electric motor weights and their maximum allowable power based on Duffy et al. [9].

The mission analysis of the motor component ultimately serves to compute the power demanded by the battery packs, $\mathbf{P}_{\text{in}}$, at all times during the mission. The way this is done is by applying efficiency penalties on the motor power output, $\mathbf{P}_{\text{out}}$, to compute the power needed by the battery packs. The power required by the battery pack is divided by the battery voltage to obtain the current draw, $\mathbf{I}$. The first efficiency penalty to consider is that of the motor itself, $\boldsymbol{\eta}_{\text{motor}}$. The motor efficiency is interpolated from a 2D efficiency map with RPM and torque as inputs. The motor map is based on data from a representative permanent magnet motor designed for high efficiency at a large range of torque and speed values[§]. The motor map is scaled to the anticipated ideal conditions of the motor. The motor operates at a constant voltage, whereas the battery pack voltage drops over time as state-of-charge decreases. To rectify this gap, a boost converter is used, which carries an efficiency penalty, $\boldsymbol{\eta}_{\text{conv}}$. The converter efficiency is computed from a 1D linear interpolation of battery voltage values given in Table 1.

[§] `https://github.com/nasa/NPSS-Power-System-Library/blob/master/include/STARCABLmotorGenerator.map`

Table 1 Converter Efficiency as a Function of Input Voltage from the Battery.

Input Voltage (V)	15	166.97	347.09	527.2	707.31	887.43	1000	1100	1300	1500
Efficiency (%)	35.89	50.97	68.91	76.68	81.35	84.81	98.36	84.81	81.35	76

After computing the efficiency values, the current draw by the motors can be computed as:

$$\mathbf{I} = \frac{\mathbf{P}_{\text{out}}}{\mathbf{V}\boldsymbol{\eta}_{\text{motor}}\boldsymbol{\eta}_{\text{conv}}} = \frac{\mathbf{P}_{\text{in}}}{\mathbf{V}}. \tag{10}$$

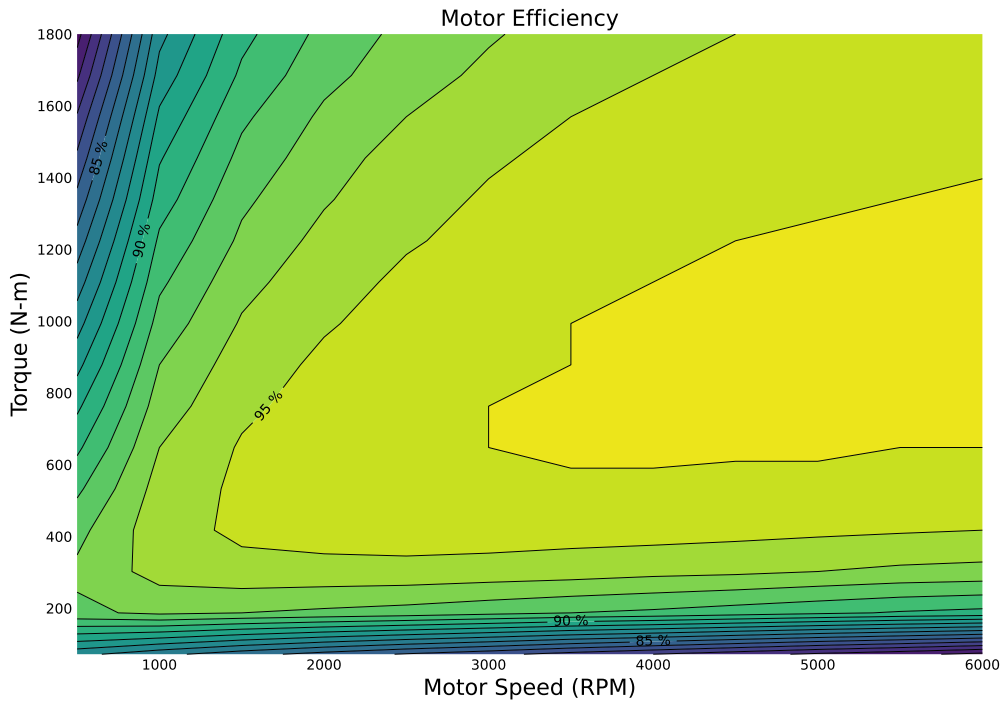

Fig. 3 Electric motor efficiency as a function of torque and speed.

III. Results

In this section, we describe the results of optimizations using Aviary with electrified propulsion using the methodology described in the previous section. All results are based on a Transonic Truss-Braced Wing (TTBW) aircraft, using similar subsystems and parameters as the work by Aretskin-Hariton et al. [3].

For the first set of results in Section III.A, we demonstrate the inclusion of electric propulsion in an Aviary-based optimization problem, and compare these results to a baseline case without electric propulsion for comparison. A full mission profile is simulated, including takeoff, climb, cruise, and descent. In the cases with hybrid-electric propulsion, 350 HP of constant electric power is added to the shaft during climb only, and the optimizer is used to size the electric motor and battery pack such that aircraft fuel burn is minimized. For cases including electric propulsion, two versions of the battery model are used: a "basic" and an "advanced" version, corresponding to the approaches described in Sections II.A.1 and II.A.2. For the advanced electrical model, we present results using two different battery cell types. Both are 18650-type cells, but differ primarily in their total energy capacity (in terms of Amp-hours) and peak discharge current. The two cell types will be distinguished by their energy capacity values: 3500 mAh and 3000 mAh.

For the second set of results in Section III.B, we vary the cell energy density of the batteries to illustrate the effect that improving cell technology would have at the conceptual aircraft level. These results are done using the advanced electric model with the 3000 mAh cell.

A. Electric Subsystem Optimization Results

Here we present optimization results of a TTBW aircraft using Aviary with additional electric propulsion using the methodology described previously in Section II. These results demonstrate the two approaches to modeling the time-dependent behavior of the battery subsystem, and compares them to a baseline case with no electrification. We encountered a surprising result with the advanced electrical model, so results using a second battery cell type are also presented for the advanced electrical model. In summary, four total models are compared:

1) No electric propulsion
2) Basic electrical propulsion model described in Section II.A.1
3) Advanced electrical propulsion model described in Section II.A.2, using 18650-type cells with 3500 mAh capacity.
4) Advanced electrical propulsion model described in Section II.A.2, using 18650-type cells with 3000 mAh capacity.

The trajectory of this optimization considers a full takeoff through landing trajectory, with a fixed 350 HP of electric power added to the turbojet shafts only during the climb phase (when electric propulsion is used). The objective function for the optimization problem is to minimize fuel burn. This will naturally lead the optimizer to minimize the mass of the electric propulsion system. For this problem, battery pack temperature is considered constant at 25 °C. The shaft speed of the electric motor is assumed to be exactly equal to the turbojet shaft speed, meaning there is no gearbox included.

For the basic electrical model, the design variables for the electric propulsion subsystem are: max motor power (P_{max}), which is a scalar value used in slack constraints on the corresponding vector-valued quantity, and nominal energy (E_{nom}), which is the total energy available in the battery pack, which is used to size the number of cells in parallel (n_{p}). For the advanced electrical model, the design variables for the electrical propulsion subsystem are: max current (I_{max}) and max motor power (P_{max}) (both of which are scalar values used in slack constraints on the corresponding vector-valued quantities), discharge rate (i_{cell}), and energy required (E_{req}). The constraints on the electric-propulsion subsystem are:

1) Battery pack state-of-charge (SOC) is greater than 20% at the end of climb.
2) The max power design variable (P_{max}) is greater than any motor power value during the mission.
3) The max current design variable (I_{max}) is greater than any current value during the mission.[¶]
4) The total energy available (E_{nom}) is greater than the energy required (E_{req}), times a factor (k) to ensure remaining state-of-charge at the end of the mission.[‖]
5) The battery pack is sized sufficiently in parallel for both peak current demand (n_{p}), as well as for total energy required for the mission ($n_{\text{p},2}$).[¶]

Finally, the optimizer is used to integrate the state variables and converge the residual equations $\mathbf{R}(\mathbf{x};\mathbf{u}) = 0$, where $\mathbf{x}$ and $\mathbf{u}$ are used as shorthand for the design variables and states, respectively. For the basic electrical model, the only state variable is energy required, E_{req}, which uses the motor power-in as the rate source. The state variables for the advanced electrical model are state-of-charge (**SOC**) and Thevenin voltage ($\mathbf{V}_{\text{Thev}}$). The full optimization problem formulations are given below in Tables 2, 3, and 4 for the baseline (no electrical propulsion), basic electrical, and advanced electrical propulsion problems, respectively.

The results of the electric-propulsion optimization problem are given below in Figure 4 and Figure 5. Figure 4 shows time histories of altitude, Mach, and throttle for the duration of the mission, and Figure 5 shows time histories of current, voltage, and state of charge during the climb phase only, since electric power is only used during climb. In both figures, values for the basic electric model are shown in blue, and values for the advanced electric model are shown in yellow and red for the 3500 mAh and 3000 mAh cells, respectively. In Figure 4, values without electrification are shown in dark gray. Also note that the x-axis values are clipped during cruise, because altitude and Mach are constant, while throttle undergoes a very gradual linear decrease, and this otherwise takes up the majority of the figure.

Figure 4 shows values of altitude, Mach, and throttle as a function of time for the duration of the mission. The profiles for each case closely resemble one another, which can be explained by the fact that the electrification is only adding 350 HP to the shaft during the climb phase, which is a small portion of the overall shaft power. Despite that, there are some noticeable changes, with the Advanced Electric: 3500 mAh model climbing the fastest due to a higher throttle setting during climb. This leads to this being the shortest duration mission overall, which may be desirable to minimize fuel burn since this case also has the highest gross takeoff weight, due to extra battery mass.

Figure 5 provides values of current, voltage, and state of charge for each model that uses electrical propulsion. Because state of charge is not integrated as a state variable in the basic model, there are no relevant values for state

[¶]Only for the advanced electrical model.

[‖]Only for the basic electrical model.

Table 2 TTBW Baseline Optimization Problem Formulation without Electric Propulsion

	Variable or Function	Size	Discipline
minimize	Fuel Burn	1	
with respect to	Design Mass Flow	1	Gas Turbine
	Gross Takeoff Mass	1	Weights
	Climb Duration	1	Trajectory
	Cruise Duration	1	
	Descent Duration	1	
	Climb Altitude	4	
	Descent Altitude	4	
	Mass	21	
	Range	21	
	Velocity	21	
subject to	Mass Residual	1	Weights
	Throttle Constraints	18	Propulsion
	Pseudospectral Constraints	67	Trajectory

of charge or current for this model, as those are not included in the basic model either. It should be noted first that these plots show straight-line interpolation between the knot points, whereas polynomial order interpolation is used for time-series integration and optimization of the model, so the jaggedness of these plots is not reflective of the model behavior. Aside from this, the overall trend is for current to increase and voltage to decrease as the mission progresses. Specifically, we see current increase from around 475 Amps to around 575 Amps at the top of climb, and voltage decrease from around 700 Volts to around 600 Volts during the same span. The pack voltage necessarily drops as state of charge drops, and so in order for the battery pack to provide the motor with enough power to output 350 HP, the current must increase to offset the voltage decrease. For the basic electric model, we assume a linearly decreasing voltage, and assume values for starting and ending voltages; in both cases, a higher voltage value was assumed, which

Table 3 TTBW Optimization Problem Formulation using the Basic Electrical Model

	Variable or Function	Size	Discipline
minimize	Fuel Burn	1	
with respect to	Design Mass Flow	1	Gas Turbine
	Gross Takeoff Mass	1	Weights
	Max Power	1	Electrical
	Nominal Energy	1	
	Energy Required	1	
	Climb Duration	1	Trajectory
	Cruise Duration	1	
	Descent Duration	1	
	Climb Altitude	4	
	Descent Altitude	4	
	Mass	21	
	Range	21	
	Velocity	21	
subject to	Mass Residual	1	Weights
	Energy Constraint	1	Electrical
	Power Constraint	12	
	Electrical Residuals	9	
	Throttle Constraints	18	Propulsion
	Pseudospectral Constraints	67	Trajectory

Table 4 TTBW Optimization Problem Formulation using the Advanced Electrical Model

	Variable or Function	Size	Discipline
minimize	Fuel Burn	1	
with respect to	Design Mass Flow	1	Gas Turbine
	Gross Takeoff Mass	1	Weights
	Max Power	1	Electrical
	Max Current	1	
	Cell Discharge Rate	1	
	Energy Required	1	
	State of Charge	9	
	Thevenin Voltage	9	
	Climb Duration	1	Trajectory
	Cruise Duration	1	
	Descent Duration	1	
	Climb Altitude	4	
	Descent Altitude	4	
	Mass	21	
	Range	21	
	Velocity	21	
subject to	Mass Residual	1	Weights
	Max Power Constraint	12	Electrical
	Max Current Constraint	12	
	Number of Cells in Parallel Constraint	1	
	State of Charge Constraint	9	
	Thevenin Voltage Constraint	9	
	Electrical Residuals	24	
	Throttle Constraints	18	Propulsion
	Pseudospectral Constraints	67	Trajectory

likely explains other discrepancies between the basic and the advanced electric models. Importantly, the Advanced Electric: 3500 mAh model only discharges to 47.4%, while the Advanced Electric: 3000 mAh model fully discharges to the 20% limit; the explanation for this follows later in this section.

Table 5 provides various values for the results of each optimization case. With no electric propulsion during climb, the optimization results in a minimized fuel burn of 16527 kg.

With a constant 350 HP of electric power added during climb, the optimized fuel burn values range from 16483-16498 kg. Table 6 shows how total fuel burn and gross takeoff weight change for each electric model type when compared to the baseline model without any electrification. Values are given in both absolute terms in kilograms, as well as on a relative percentage basis. Using the basic electrification model, we see a reduction in total fuel burn by 44.07 kg, or 0.267%. When we move to the advanced electric model (with 3500 mAh) cells, we see a fuel burn reduction in only

Table 5 Optimization Results

Electric Type	Fuel Burn (kg)	GTOW (kg)	Battery Mass (kg)	Cell Energy Density (Wh/kg)	Motor Mass (kg)	Motor Max Power (kW)	n_s	n_p (%)	SOC Final
None	16527	134931	-	-	-	-	-	-	
Basic	16483	136588	639.6	264.4	97.9	261	-	-	20
Advanced: 3500 mAh	16524	137592	1055.9	264.4	97.9	261	172.4	52.3	47.4
Advanced: 3000 mAh	16498	137058	836.3	225	97.9	261	172.4	38.9	20

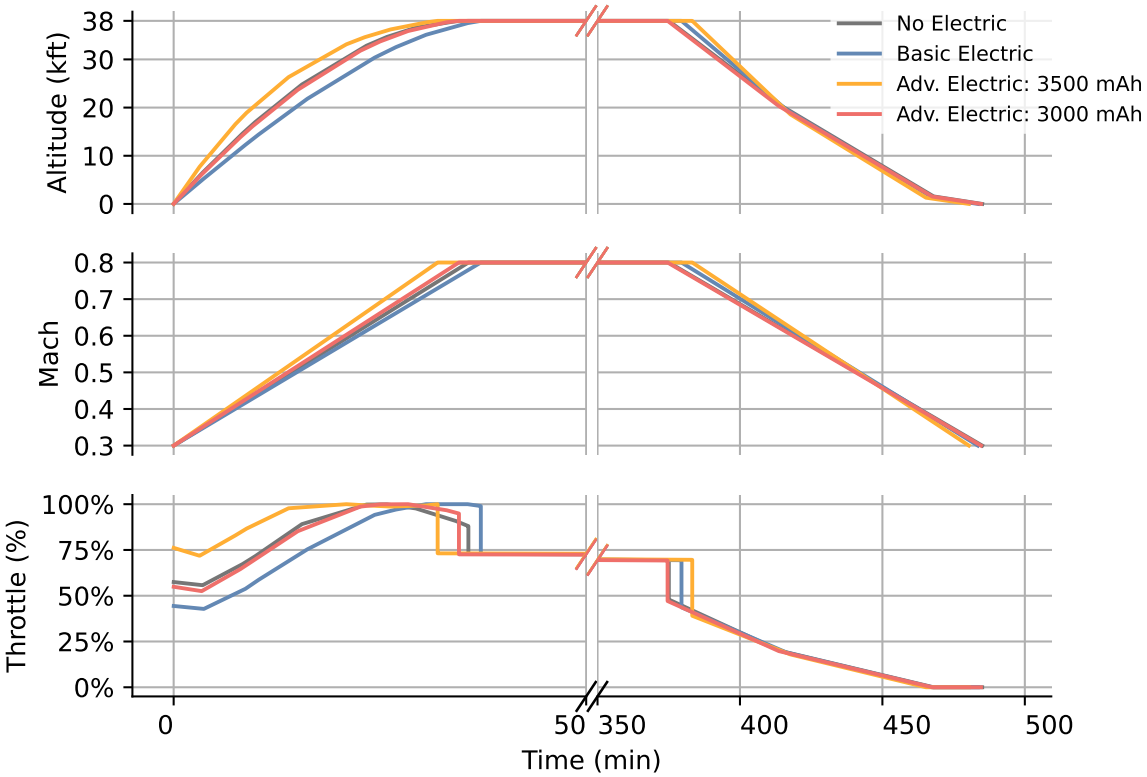

Fig. 4 Summary of the resulting mission for each model.

Table 6 Changes in fuel burn and gross takeoff weight (GTOW) compared to the baseline without electrification.

Electric Type	Fuel Burn Reduction	GTOW Increase
Basic	44.07 kg (0.267 %)	1657.0 kg (1.228 %)
Advanced: 3500 mAh	2.87 kg (0.017 %)	2661.4 kg (1.972 %)
Advanced: 3000 mAh	29.43 kg (0.178 %)	2126.6 kg (1.576 %)

2.87 kilograms. This is a surprising result, but there is a good reason for this; in Table 5, we can see the the final state of charge for this model is at 47%. This is because the number of cells in parallel (n_p) is sized to meet two constraints: the total energy of the battery, and also the peak current demand (our I_{max} slack constraint). In the case of the basic electric model, the number of cells in parallel is only sized to meet the total energy demand, but the constraint becomes active when we move to the advanced electric model. The first cell we started with was an 18650-type cell with 3500 mAh of energy, and a maximum current of 10 Amps. By changing the cell type slightly to a different type of 18650 cell, we can achieve better results with this model. By changing the 18650 cell to one with 3000 mAh of energy, but a higher maximum current of 15 Amps, the final state of charge now hits the lower bound of 20%. By changing the cell type, the fuel burn reduction is now 29.43 kg, or 0.178% of the total fuel burn. This is more closely aligned with the basic electrical model as well.

In the case of the basic electric model, the fuel burn reduction of 44.07 kilograms comes at the expense of a 1657

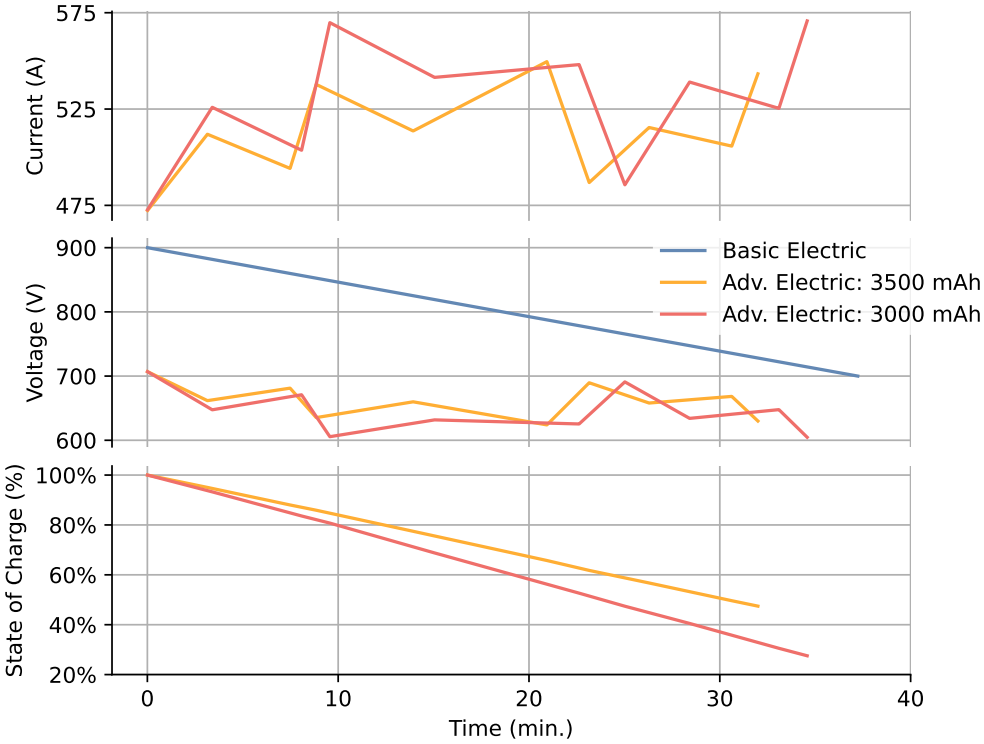

Fig. 5 Electric-subsystem behavior during an optimized climb segment.

kilogram increase in gross takeoff weight, due to the addition of the battery packs and electric motors. Using the advanced electric model with the 3500 mAh cells, we see a 2661.4 kilogram increase in gross takeoff weight. This explains the result we saw with the fuel burn only being reduced by 3 kilograms; the additional mass required by the electrical subsystem almost fully offsets the additional electric power added to the shaft, in terms of fuel burn savings. In this case, the 47% state of charge remaining at the end of the mission means that additional fuel is needed to carry batteries that do not expend any energy. After switching the cell type to a different version of the 18650 cell with a higher max current, the optimization switches back to sizing the number of cells in parallel based on the total energy requirement, rather than the peak current requirement. This means that the pack can be discharged to the 20% limit, resulting in the aircraft not carrying as much extra weight as in the case with 3500 mAh cells. This highlights the importance of selecting the proper cell type for a mission, and for this decision being a point of emphasis for electric propulsion concepts.

B. Trends in Increasing Cell Energy Density

The optimization results using electric propulsion in Section III.A assume battery cell energy density values representative of technology available today. Here, we investigate the impact that advancing battery technology would provide at the conceptual aircraft level. Figure 6 shows the optimized fuel burn value using when cell energy density is increased to varying degrees. These results are somewhat limited, in that we applied the same optimization problem formulation that we used for the previous results in Section III.A, with a fixed 350 HP electric shaft power applied during climb only. By constraining the electric shaft power to a fixed amount, the optimizer does not have the freedom to request more electric power, even as it becomes more favorable to do so. Additionally, by only applying the electric shaft power during climb, the overall impact of increasing the cell energy density will be mitigated. For each of these problems, we apply the advanced electric model with 3000 mAh cells, and simply decrease the mass of each cell in order to obtain the desired value of cell energy density. The initial value of cell energy density of 225 Wh/kg is the value used in the previous results in Section III.A. From there, we test cell energy density values between 300 Wh/kg and 900 Wh/kg, in increments of 100. 900 Wh/kg represents a cell energy density four times the baseline value, a considerable gap. However, for the modeling assumptions made here, we see the largest decrease in total fuel burn with the initial increases in cell energy density. By increasing cell energy density from 225 Wh/kg to 300 Wh/kg, we see a total fuel

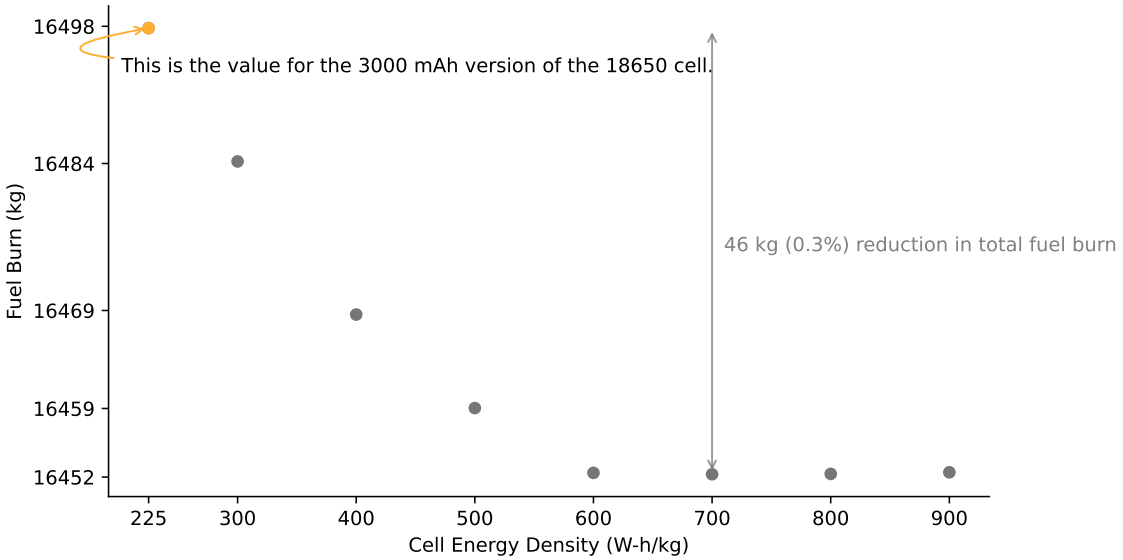

Fig. 6 Total fuel burn for the mission with varying cell energy density.

burn decrease of 14 kg. This is significant for this problem, considering that the fuel burn savings in going from the baseline model with no electrification to the advanced electric model is 29.4 kg. By 600 Wh/kg, the fuel burn benefits are no longer noticeable. Again, this is limited by the optimization problem formulation we used, but this shows a 46 kg decrease in fuel burn can be obtained by increasing cell energy density from 225 Wh/kg to 600 Wh/kg, which is a significantly larger fuel burn decrease than we saw from adding electrification to the baseline model. Another reason for the asymptotic behavior of this trend, is that this follows the $1/x$ decreasing trend of cell mass that we apply to obtain the increase in cell energy density. In other words, by the time we get to 600 Wh/kg cell energy density, we are applying electric energy without any noticeable mass penalty; decreasing the mass further does not help, because it is already a small fraction of gross takeoff weight at this point. The optimal fuel burn of 16452 kilograms represents the fuel burn required to run the full mission, and the weight of the battery pack for this amount of electric power is negligible for any value greater than this. The benefit of increasing cell energy density could be utilized more effectively with alternate problem formulations that should be studied in future work. An additional consideration is that as cell energy increases, the fraction of pack weight should increase, due to the thermal management and safety requirements of the pack [2].

IV. Conclusion

In this work, we presented an electric propulsion model consisting of a battery pack model including cell-level discharge connected to a converter and electric motor model, and applied this to Aviary. We demonstrated this electric propulsion model by comparing four optimizations of the same configuration and mission: a baseline case without electric propulsion, and three versions of the electric propulsion model.

These results showed that the addition of electric shaft power during climb can reduce total fuel burn by between 29 and 44 kilograms for this specific problem formulation using battery technology available today. We also importantly demonstrated that the initial cell type that we selected was not compatible with this configuration, almost fully negating the benefit of adding electric propulsion, and that making a small change to the cell type can have a large impact at the system level. Finally, we compared optimal fuel burn values for a range of cell energy densities to show what impact improving battery technology can have for this type of hybrid electric propulsion system.

Acknowledgements

The work presented in this paper was developed with support from NASA's Transformational Tools and Technologies (TTT), Advanced Air Transport Technology (AATT), and Electric Powered Flight Demonstration (EPFD) Projects. These projects are funded by the Transformational Aeronautic Concepts Program (TACP), Advanced Air Vehicles Program (AAVP), and Integrated Aviation Systems Program (IASP) respectively. Funding for those Programs is provided by the Aeronautic Research Mission Directorate (ARMD).

References

[1] Chin, J., Schnulo, S. L., Miller, T., Prokopius, K., and Gray, J. S., "Battery performance modeling on SCEPTOR X-57 subject to thermal and transient considerations," *AIAA Scitech 2019 Forum*, San Diego, CA, 2019. doi:10.2514/6.2019-0784, AIAA 2019-0784.

[2] Chin, J. C., Look, K., McNichols, E. O., Hall, D. L., Gray, J. S., and Schnulo, S. L., "Battery Cell-to-Pack Scaling Trends for Electric Aircraft," *2021 AIAA/IEEE Electric Aircraft Technologies Symposium (EATS)*, Virtual, 2021. doi:10.23919/EATS52162.2021.9704819, AIAA 2021-3316.

[3] Aretskin-Hariton, E., Gratz, J., Jasa, J., Moore, K., Falck, R., Kuhnle, C., Leader, M., Chapman, J., and Hendricks, E., "Multidisciplinary Optimization of a Transonic Truss-Braced Wing Aircraft using the Aviary Framework," *AIAA SciTech 2024 Forum*, Orlando, FL, 2024. doi:10.2514/6.2024-1084, AIAA 2024-1084.

[4] Gratz, J., Jasa, J., Aretskin-Hariton, E., Moore, K., Marfatia, K., Kirk, J., and Recine, C., "Aviary: An Open-Source Multidisciplinary Design, Analysis, and Optimization Tool for Modeling Aircraft with Analytic Gradients," *AIAA Aviation 2024 Forum*, Las Vegas, NV, 2024.

[5] Gray, J. S., Hwang, J. T., Martins, J. R. R. A., Moore, K. T., and Naylor, B. A., "OpenMDAO: An open-source framework for multidisciplinary design, analysis, and optimization," *Structural and Multidisciplinary Optimization*, Vol. 59, No. 4, 2019, pp. 1075–1104. doi:10.1007/s00158-019-02211-z.

[6] Falck, R., Gray, J. S., Ponnapalli, K., and Wright, T., "dymos: A Python package for optimal control of multidisciplinary systems," *Journal of Open Source Software*, Vol. 6, No. 59, 2021, p. 2809. doi:10.21105/joss.02809.

[7] Gill, P. E., Murray, W., and Saunders, M. A., "SNOPT: An SQP algorithm for large-scale constrained optimization," *SIAM Review*, Vol. 47, No. 1, 2005, pp. 99–131. doi:10.1137/S0036144504446096.

[8] Lambe, A. B., and Martins, J. R., "Extensions to the design structure matrix for the description of multidisciplinary design, analysis, and optimization processes," *Structural and Multidisciplinary Optimization*, Vol. 46, 2012, pp. 273–284. doi:10.1007/s00158-012-0763-y.

[9] Duffy, M., Sevier, A., Hupp, R., Perdomo, E., and Wakayama, S., "Propulsion scaling methods in the era of electric flight," *2018 AIAA/IEEE Electric Aircraft Technologies Symposium (EATS)*, IEEE, Cincinatti, OH, 2018, pp. 1–23. doi:10.2514/6.2018-4978, AIAA 2018-4978.